Hindawi
Mathematical Problems in Engineering
Volume 2019, Article ID 5713602, 14 pages
https://doi.org/10.1155/2019/5713602

Research Article

Flotation Height Prediction under Stable and Vibration States in Air Cushion Furnace Based on Hard Division Method

Shuai Hou[1], **Jianhui Liu**[1] and **Wu Lv**[2]

[1]*School of Information and Electrical Engineering, Hebei University of Engineering, Handan, Hebei 056038, China*
[2]*School of Information Science & Engineering, Northeastern University, Shenyang, LiaoNing 110004, China*

Correspondence should be addressed to Wu Lv; lvwu@ise.neu.edu.cn

Received 8 July 2019; Accepted 26 November 2019; Published 13 December 2019

Academic Editor: Arkadiusz Zak

Air cushion furnace is indispensable equipment for the production of high quality strip, and it is significant to national economy. The flotation height is a key factor to the quality and efficiency of the product. However, the current prediction models can merely predict the flotation height of strip in air cushion furnace at single working state. The precision of prediction model is inaccurate at the circumstance of low flotation height. To solve the above problem, firstly, this paper proposes a framework which can predict the flotation height of strip under both stable and vibration states. The framework is composed of the hard division model and prediction model. Secondly, a hard division method is proposed based on clustering which combines stacked denoising autoencoder and floating process knowledge. Thirdly, a parallel hybrid flotation height prediction model is proposed, which can provide desirable prediction results at the circumstance of low flotation height. Finally, the LSSVR model is used to predict the maximum and minimum flotation height of strip at vibration state. The experimental results show that the framework can accurately divide the stable and vibration states of the strip and can accurately predict the flotation height of the strip under the stable and vibration states. The research contents of this paper lay an important theoretical foundation for the precise process control in air cushion furnace.

1. Introduction

In view of the high surface quality requirements of the high quality strip product, air cushion furnace is indispensable equipment for heat treatment in the production process of the high quality strip product [1, 2]. In comparison with the traditional heat treatment furnace, air cushion furnace is characterized by the following advantages: (a) the strip is suspended in the air for drying so that scratch on the strip is avoided by this noncontact drying manner and (b) air cushion furnace owns higher production efficiency [3, 4].

Flotation height of the strip in the air cushion furnace is a key factor to the surface quality of the strip. It should be emphasized that the flotation height expresses the floating height of the strip in this paper. The meaning of flotation height in this paper is different to flotation height in mineral processing [5, 6]. When the flotation height of the strip is too high or too low, the strip will contact with equipment and further be scratched. This leads to the scenario that the product surface quality cannot meet the production requirements. In addition, the flotation height of the strip greatly affects the heating rate and cooling rate. So, the related research of flotation height is significant [7].

In the actual operation process of air cushion furnace, some problems exist in the flotation process, such as complex operating conditions, coexistence of steady and vibration working conditions, difficulty in obtaining label data, and strong interference in production process. Prediction accuracy degree of the flotation height under stable state and vibration state is a key restricting factor for the process control of air cushion furnace. Therefore, it is of great significance for the production process control of air cushion furnace to study the prediction model of the strip flotation height in air cushion furnace under stable and vibration states [8, 9].

Stable state and vibration state coexist in the production process of the air cushion furnace. The strip is floated stably in air under stable state while the strip is fluttering in air

under vibration state. For the above reasons, we propose a flotation height prediction model based on the hard division method, which can further divide the working states into stable state and vibration state [1, 10].

Recently, there have been some relevant research works on the problem of flotation height prediction of strips under stable state based on the experimental data via the air flotation experimental platform. Chen et al. predicted the flotation height of strip under stable state by using the data fitting method [11]. Moretti combined the axially moving beam, thin-wall jet theory, and thick-wall jet theory with other ground effect models to establish a mechanism flotation height prediction model of the strip in the air flotation furnace [12]. Hou et al. proposed a parallel hybrid flotation height prediction model, i.e., SBEH, which is composed of the mechanism prediction model and the data error compensation model. The proposed model combined the high generalization performance of the mechanism model with the strong learning ability of the data-driven model [1]. However, the flotation height of the strip was usually low at stable state. Existing flotation height hybrid models under stable state were established on thin-wall jet theory. Some studies have also proved that the thin-wall jet theory is less efficient than thick-wall jet theory in the low flotation height circumstance [10]. To the best of authors' knowledge, a flotation height hybrid model based on the thick-wall jet theory has not been reported in the literature.

In addition to the stable state, the flotation height prediction of strip under vibration state has also attracted the attention of some scholars. Cho established a vibration model for the first four modes of strip on the basis of the eigenvalue method, the linear gyroscopic system principle, and the discrete system principle. Moreover, the stable state and vibration state of the strip also have been divided and recognized by artificial experience [13]. Takeda and Watanabe et al. used experimental data and expert experience to construct a vibration prediction model of conveyer belts under self-excited vibration state [14]. The vibration process of the strip in the air-cushion furnace belongs to the fluid-solid coupling process so that it is often difficult to establish the mechanism model of the strip vibration. Furthermore, mechanism models generally use some physical assumptions as an ideal precondition, which lead to the prediction results failing to meet the precision requirement in industrial process. The highest and lowest flotation points of strip are most likely to contact with nozzles and be scratched. Therefore, in order to ensure the quality of the strip, accurately predicting the strip height is a key issue. With the development of the machine learning methods, the data-driven model has achieved good effects on the prediction of vibration signal in other industrial fields. Jiang et al. used a machine learning model with sinusoidal input signal to predict the magnitude and frequency of forced vibrations in the power system [15]. Multiple machine learning algorithms were employed to predict process parameters of drought crisis, such as the severity, duration, and peak intensity of drought. The experimental results showed that the LSSVR model has achieved good prediction results [16]. So far, it has not been found to utilize the data-driven method to predict the highest and lowest points of the flotation height under the vibration state.

At present, the existing research studies can either establish the flotation height model under stable state or vibration state. Due to the significant difference between stable state and vibration state, a single model is hard to predict the flotation height under both stable state and vibration state accurately. Some scholars have successfully divided the process into several different stages and established the submodels at each stage in related industry field [17, 18].

The k-means method was used to divide different working modes in the industrial process. For the division of states, Qin et al. and Zhao used the k-means method to divide the injection modeling process of polymer into several states [17, 18]. However, three shortcomings exist in the traditional k-means method. Firstly, the k-means method divides the dataset into k different cluster sets, but it cannot determine which category of a cluster set belongs to? Secondly, the initial center points of k-means are difficult to be determined. Finally, the generalization performance of the k-means model is poor. Previous studies have shown that adding additional empirical knowledge or constraints to the training process of the data-driven model can effectively improve the generalization performance of the data-driven model [19–21]. To extract the information of the process, Zhao used the PCA method to extract the process information of the production process [18]. Hu compared the information capture ability between the PCA and the autoencoder in transition process. The autoencoder method shows strong processing ability in the process of information extraction. The result shows that autoencoder can well capture the important information of production transition process [22]. Deng et al. suggested that the autoencoder owned better nonlinear feature extraction ability than the PCA method. An autoencoder can effectively utilize potential information to improve the prediction accuracy of a classifier [23]. In addition, the industrial process often includes nonlinear process and contains lot of outliers. In order to suppress the noise and outliers in the industrial field data, some scholars have used the denoising autoencoder to extract process information. Gong et al. used the sparse denoising autoencoder to extract feature information from dataset containing outliers and got desirable prediction results [24].

For the above reasons, it is vital to establish a division model which can consider the air flotation process knowledge and improve the predictive performance of flotation height. Firstly, this paper proposes a framework which can predict the flotation height at both stable state and vibration state. This frame is based on the hard division method. It can divide the flotation states and predict the flotation height under stable state and vibration state. Secondly, a hard division method combining stacked denoising autoencoder and floating process knowledge based clustering is presented. It can divide the work condition into steady state and vibration state. Thirdly, we propose a parallel hybrid flotation height prediction model for stable state via the simplified mechanism model and data error compensation model. Finally, a flotation height model is used to predict the maximum and minimum flotation height under vibration state.

Specifically, the contributions of this paper can be summarized as follows: (a) the framework can predict the flotation height of strip under both stable and vibration states, and (b) this paper combines the k-means method with production process knowledge to build a hard division model, and (c) we propose a parallel hybrid flotation height prediction model for stable state.

The remainder of this paper is organized as follows. Section 2 briefly introduces the working process of air cushion furnace and related works. Section 3 height prediction model based on hard division method. Section 4 reports the experimental results and discussion. Section 5 draws conclusions.

2. Related Background and Algorithm

2.1. Related Background. In the production process, the strip is floated in the air without contacting with equipment. The production process of the air cushion furnace is shown in Figure 1.

As shown in Figure 1, the air cushion furnace has upper and lower rows of air boxes, respectively, arranged into two slot nozzles. The air goes into the air box from the inlet and goes out the air box from the slot nozzle. Then, the air impinges the upper and lower surfaces of the strip. The lower slot nozzles produce impinging force F_1 on the lower surface of the strip, and the upper slot nozzles produce impinging force F_2 on the upper surface of the strip. The strip will be suspended in the air when the value of F_1 minus F_2 is equal to the value of the gravity of the strip. During the production process of the air cushion furnace, the strip has two flotation states: stable state and vibration state.

The floating state of the strip is related to the fluid density, the impinging angle of the upper and lower slot nozzles, the upper and lower nozzle pressure, the thickness of the strip, and the density of the strip. The impinging angles of the upper and lower nozzles are determined by the equipment structure. The thickness and the density of the strip are the same in the same batch. Thus, the main influence factors of flotation height are the upper nozzle pressure and the lower nozzle pressure. The relationship between the nozzle pressure and flotation state of strip is shown in Figure 1(a). The solid line in the Figure 1(a) divides the flotation state of strip into stable state and vibration state. The horizontal axis represents the pressure P_{t1} of the lower nozzle, and the vertical axis represents the pressure P_{t2} of the upper nozzle. In general, the greater the lower nozzle pressure P_{t1} is, the more easily the strip enters to the vibration state when P_{t2} is fixed. The greater the upper nozzle pressure P_{t2} is, the more easily the strip enters to the vibration state when P_{t1} is fixed. Stable floating state of strip in Figure 1(a) is shown in Figure 1(b). The strip floats stably at a certain height at Phase I. Vibration flotation state of strip in Figure 1(a) is shown in Figure 1(c). The strip oscillates around a certain position at Phase II.

In Figure 1(b), V_j is the air impinging velocity of the nozzle, w is the distance between two slot nozzles, b is the width of a single slot nozzle, h is the flotation height of the strip, θ is the impinging angle of the slot nozzle, and d is the distance between the lower edge of the upper nozzle and the upper edge of the lower nozzle.

2.2. Stack Denoising Autoencoder. Stack denoising autoencoder (SDAE) is a mature algorithm, which stacks the denoising autoencoders to extract feature.

$$\mathbf{s}_i = \sigma_L\left(\sigma_{L-1}\left(\ldots\sigma_l\left(\mathbf{W}_l\mathbf{x}_i + \mathbf{b}_l\right)\right)\right), \tag{1}$$

where $\mathbf{x}_i$ is the i-th sample in dataset X, $\mathbf{W}_l$ is weight matrix between input nodes and hidden nodes in the l-th denoising autoencoder, $\mathbf{b}_l$ is bias vector in hidden nodes of the l-th denoising autoencoder, $l = 1, \ldots, L$. $\sigma(\cdot)$ is the *sigmoid* activation function, L is the layer number of SDAE, and $\mathbf{s}_i$ is the final features extracted by activation function. This paper uses the classical SDAE algorithm, which can be found in [25]. In view of the favorable data mining ability of SDAE on noisy data in industry field, the SDAE is used to extract the information from the process data of air cushion furnace.

2.3. k-Means. The k-means algorithm divides a dataset into K clusters according to distance between samples [26]. C_i is the i-th cluster. Minimizing the square error E is given by

$$E = \sum_{i=1}^{k} \sum_{x \in C_i} \left\| x - \mu_i \right\|_2^2, \tag{2}$$

where μ_i is mean vector of C_i, also known as barycenter. The equation of μ_i can be formulated as

$$\mu_i = \frac{1}{|C_i|} \sum_{x \in C_i} x. \tag{3}$$

3. Flotation Height Prediction Model Based on Hard Division Method

3.1. Hard Division Method Based on Autoencoder and Empirical Clustering. The k-means method has some problems: (a) the initial center points are difficult to be determined, (b) the parameter K needs to be manually adjusted, and (c) the class of subcluster is hard to be determined after clustering. However, the actual production process of air cushion furnace is a time continuous process, and the number of clusters K is difficult to be determined.

For the above problems of the k-means method, this paper proposes a floating process knowledge based on the clustering method and the empirical knowledge of flotation process, which is a hard partition method based on autoencoder and empirical clustering (HPAEC).

3.1.1. Floating Process Knowledge-Based Clustering. The state division of experience is an extensive division method. Due to the fact that it is greatly affected by artificial experience, we cannot guarantee the accuracy of division results.

In order to improve the accuracy of the division result of stable state and vibration state, a new state division method

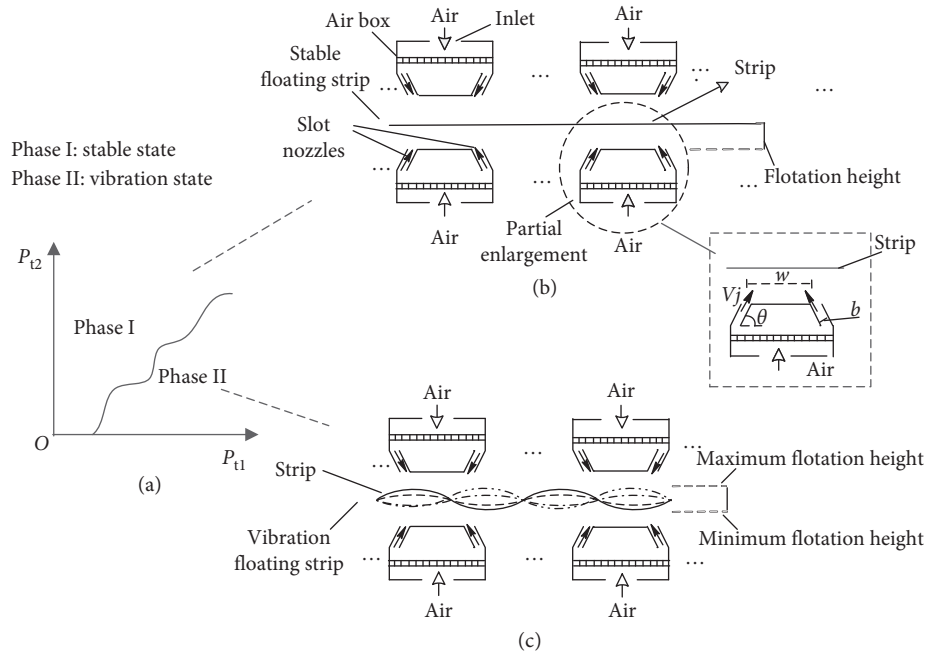

Figure 1: Schematic diagram of stable state and vibration state.

combined floating process knowledge is proposed. This method exactly divides the flotation state based on the extensive division results of the state division of experience. For illustration convenience, floating process knowledge-based clustering algorithm is named as FPKC in the following. FPKC algorithm is shown in Figure 2.

In Figure 2(a), the horizontal axis represents the lower nozzle pressure P^*_{t1}, and the vertical axis represents the upper nozzle pressure P^*_{t2}. P^*_{t1} and P^*_{t1} are transformed from P_{t1} and P_{t2} by SDAE. Based on the flotation test of air cushion furnace by the cross-validation experiment, the solid line ② of Figure 2(a) which represents the curve of state division of experience is obtained. With the increase of P^*_{t1} and the decrease of P^*_{t2}, the state of the strip is more likely to be the vibrate state. Moreover, with the increase of P^*_{t2} and the decrease of P^*_{t1}, the state of the strip is more likely to be the stable state.

Due to inaccuracy of the state division of experience method, a region around the curve ② at interval of d is obtained; in other words, the region named as fuzzy region is between ① and ③. $Co1$ is the geometric center points of labeled experimental data distributed on the upper left part of curve ①, and $Co2$ is the geometric center points of labeled experimental data distributed on the lower right part of curve ③. The hard division method procedure is given in Figure 3, and the detailed descriptions are shown as follows (Algorithm 1).

For illustration purposes, in Figure 2, Line1 represents an operation track. The variables X^*_n, T^*_i, P^*_{t1}, P^*_{t2}, $Cto1$, and $Cto2$ are transformed from X_n, T_i, P_{t1}, P_{t2}, $Co1$, and $Co2$ by SDAE. In Figure 2(a), in Step 1, starting point numbering of line1 is set as T^*_1. The intersection point numberings of the curve Line1 and curve ①, ②, ③ are T^*_2, T^*_3, and T^*_4. The end point numbering of line1 is T^*_5. In Step 2, line 1 is divided into the line segment $\{T^*_1\text{-}T^*_2\}$, $\{T^*_2\text{-}T^*_3\}$, $\{T^*_3\text{-}T^*_4\}$, and $\{T^*_4\text{-}T^*_5\}$. Then, the line segments are defined as cluster $\{C^*_1, C^*_2, C^*_3, C^*_4\}$. In the Figure 2(b), after the cluster center adjustment, cluster merging, and sample assignment in Step3, Step4, Step 5, and Step6, the clusters in Line1 are changed to $\{T^*_1\text{-}T^*_6\}$ and $\{T^*_6\text{-}T^*_5\}$. $\{T^*_1\text{-}T^*_6\}$ is closer to $Cto1$, so it is divided into the stable state. $\{T^*_6\text{-}T^*_5\}$ is closer to $Cto2$, so it is divided into vibration state.

3.1.2. Experience Hard Division Method of SDAE. The experience hard division method combines the FPKC with the SDAE. The flowchart is shown in Figure 4. In Figure 4, the SDAE extracts data features from the input dataset $\{X, Y\}$, and then FPKC divides input dataset $\{X, Y\}$ into stable state dataset $\{X^S, Y^S\}$ and vibration state dataset $\{X^V, Y^V\}$ based on extracted data features.

3.2. Stable State Prediction Model (SSPM). In this section, we propose a parallel hybrid prediction model based on mechanism model and data-driven model. The mechanism model is based on thick-wall jet theory and gravity balance equation, while LSSVR is employed as the error compensation model to predict the error and unmodeled parts of the mechanism model. The structure of the hybrid prediction model of strip is shown in Figure 5.

The main information of flotation height is predicted by the mechanism model. The nonmain information of flotation height and the unmodeled part of the mechanism model are compensated by the data-driven model. The structure of the parallel hybrid prediction model is shown in Figure 5. The details are provided as follows:

(1) Online data collection: on the existing experimental device, the experimental dates $\{X^S, Y^S\}$ in stable flotation process are collected by online sensors. X^S is

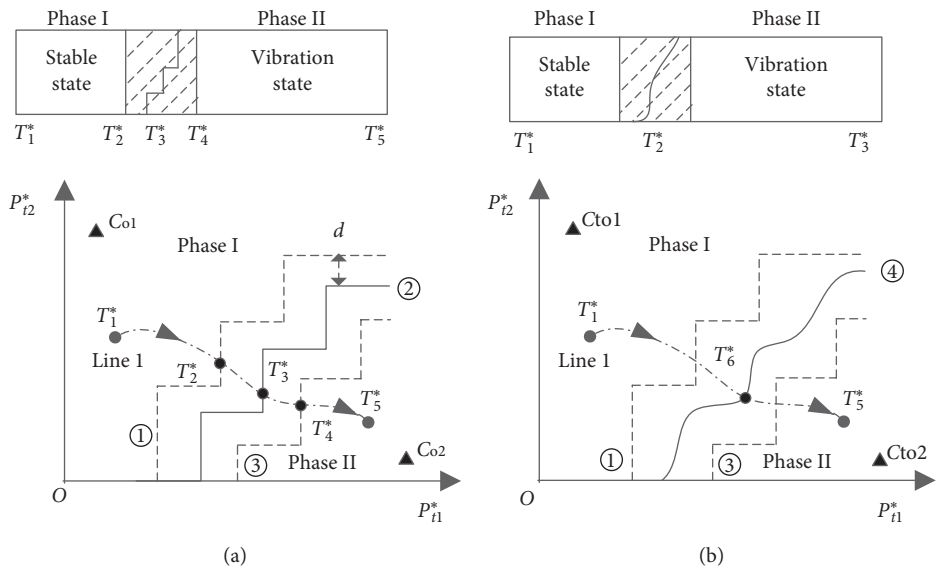

Figure 2: Hard division schematic diagram. (a) Extensive division phase. (b) Fine division phase.

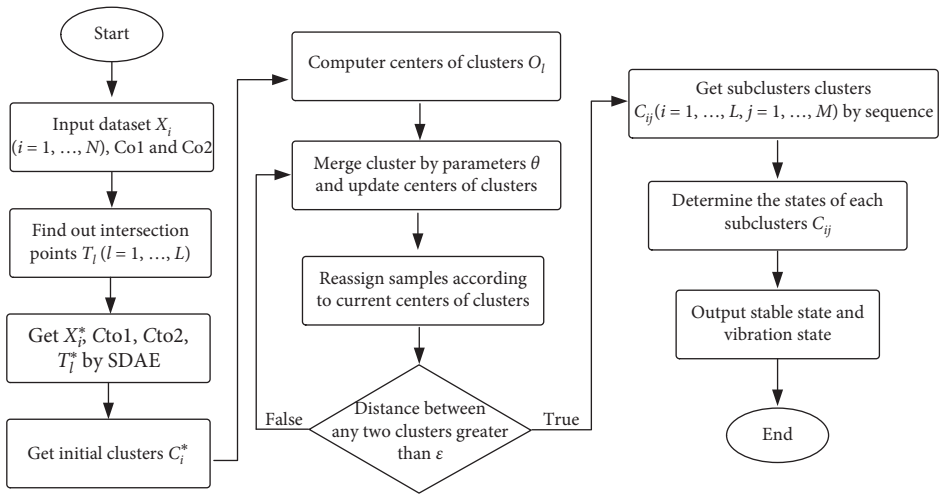

Figure 3: The design flowchart of hard division.

the feature of data and Y^S is actual value of flotation height in stable state, which are online tested by laboratory.

(2) Mechanism mode: the stable state dataset $\{X^S, Y^S\}$ is provided to the mechanism model which outputs the flotation height. X^S is the feature data of flotation height and e^s is the error between the mechanism model and actual value. X^S and e^S constitute the error compensation dataset $\{X^S, e^S\}$.

(3) Data error compensation model: the error compensation model LSSVR is trained by the error compensation dataset $\{X^S, e^S\}$ and outputs the error compensation value.

The final prediction value of the flotation height is obtained by fusing the outputs of the mechanism model and the LSSVR data-driven model.

3.2.1. Stable State Flotation Height Mechanism Model. In previous studies, the flotation height prediction model of stable state is built on the thin-wall jet theory. The applicable condition of the thin-wall jet theory is $b/h \ll 1$. In other words, this theory is suitable for circumstance where the flotation height of strip is high. However, applicable condition of the thick-wall jet theory is $h/b \leq 4$. That means thick-wall jet theory is suitable for circumstance where the flotation height of strip is low. However, in the actual production process, the flotation height of strip usually is low when the strip is under stable state. Therefore, the thick-wall jet theory is more suitable for stable state flotation height prediction [10].

The thick-wall jet theory has a prerequisite assumption: due to the effect of centrifugal force, there is a pressure gradient field with uniform change in the thin-layer profile of air cushion [10]. The requirements of force balance are

Input: geometric center points $Co1$ and $Co2$, operation process training dataset $X = \{X_1, \ldots, X_N\}$, Line 1 represents X; x_i is a time slice data presenting a point of Line 1. Time slice representing a vector includes all features at a fixed time.
Output: stable state and vibration state.
Step 1: The variables $\{X_i, T_l, Co1, Co2\}$ are transformed into $\{X_i^*, T_l^*, Cto1, Cto2\}$ utilizing SDAE.
Determine the number of the intersection points N of the curve Line 1 and curve ①, ②, ③. The starting point numbering of Line1 is set as T_l^*. Along the trajectory direction of Line1, set intersection points numbering as T_l^* $(l = 2, ..., L)$. The end point numbering of Line 1 is T_{L+1}^*.
Step 2: All time slices in interval $[T_l^*\text{-}T_{l+1}^*]$ are set as cluster C_l^*; $l = 1, ..., N$. O_l^* is the mean value of all samples in C_l^*, $l = 1, ..., N$; and O_l is also the center of cluster C_l^*.
Step 3: For all clusters, any two clusters are merged, if the Euclidean distance between two centers of clusters is smaller than θ. The center of the merged cluster is recalculated.
Step 4: Each sample in X is compared to each centroid of each cluster and assigned to the cluster whose centroid is nearest. Update all of the cluster centers. Calculate the distance between the original cluster center and the updated cluster center. If the distance is less than a minimum clustering distance threshold ε, go to Step 5. Otherwise, return to Step 3 and $O_l^* = O_l^{*\prime}$, $O_l^{*\prime}$ is the updated center of cluster C_l^*.
Step 5: The time discontinuous data in C_i are sorted by time sequence and are divided into M_i different subclusters. The different subclusters are described as C_{ij}, where $j = 1, 2, \ldots, M_i$.
Step 6: For all C_{ij}, if dist $(Cto1, C_{ij}) <$ dist $(Cto2, C_{ij})$, C_{ij} belongs to stable state; otherwise, C_{ij} belongs to vibration state.

Algorithm 1

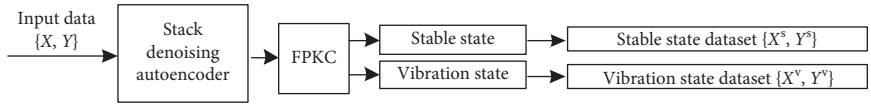

Figure 4: The flowchart of hard division.

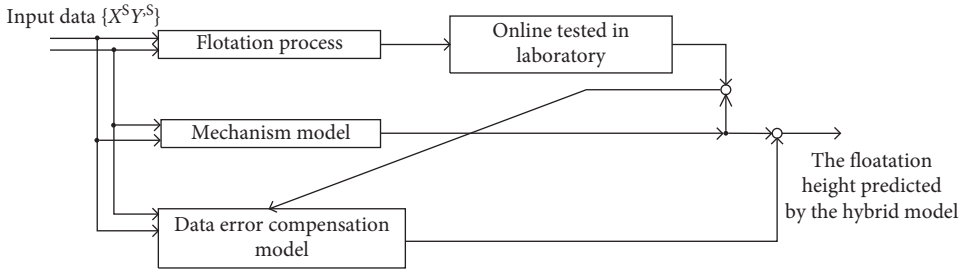

Figure 5: Schematic diagram of stable state flotation height model.

$$V_j^2 = \frac{p_c h}{\rho b (1 + \cos\theta)}, \tag{4}$$

where ρ is air density, b is width of slot nozzle, V_j is air impinging velocity, p_c is the air cushion pressure, and θ is impinging angle of nozzle.

The equation of thick-wall jet theory is

$$p_c = \left[1 - \left(\frac{(h/b) - 1}{(h/b) + \cos\theta}\right)^2\right] \cdot P_t, \tag{5}$$

where P_t is nozzle pressure and b is width of slot nozzle.

According to equation (5),

$$p_{c1} = \left[1 - \left(\frac{(h/b) - 1}{(h/b) + \cos\theta}\right)^2\right] \cdot P_{t1}, \tag{6}$$

$$p_{c2} = \left[1 - \left(\frac{((d-h)/b) - 1}{((d-h)/b) + \cos\theta}\right)^2\right] \cdot P_{t2}, \tag{7}$$

where h is the flotation height, p_{c1} and p_{c2} are defined as air cushion pressure of under surface and upper surface of strip, p_{t1} and p_{t2} are the pressures of the lower and upper air box, and d is the distance between the lower edge of the upper nozzle and the upper edge of the lower nozzle.

Air impinging force per unit length is

$$F = p_c w + 2\rho b V_j^2 \sin\theta, \tag{8}$$

where w is distance between the slot nozzles. Substituting equations (4), (6), and (7) into equation (8):

$$F_1 = n_1 P_{c1} \cdot \left[w + \frac{2h \cdot \sin\theta}{1 + \cos\theta} \right], \tag{9}$$

$$F_2 = n_2 P_{c2} \cdot \left[w + \frac{2(d-h) \cdot \sin\theta}{1 + \cos\theta} \right], \tag{10}$$

$$F_1 - F_2 = G, \tag{11}$$

where the strip exerts upward force F_1 and downward force F_2, n_1 and n_2 are the number of the lower and upper air box respectively, and G is gravity of the strip.

Flotation height h is obtained by solving the coupled equations of (9), (10), and (11).

$$Ah^4 + Bh^3 + Ch^2 + Dh + E = 0, \tag{12}$$

where the parameters A, B, C, D, and E are expressed as equations (13)–(17):

$$A = 4b \sin\theta (n_1 P_{t1} - n_2 P_{t2}) - G, \tag{13}$$

$$\begin{aligned} B = {} & \left[2b^2 \sin\theta (\cos\theta - 1) + 2wb(\cos\theta + 1) \right. \\ & \left. - 8b^2 \cos\theta \sin\theta \right] (n_1 P_{t1} + n_2 P_{t2}) \\ & + 8db \sin\theta (n_2 P_{t2} - n_1 P_{t1}) + 2dG, \end{aligned} \tag{14}$$

$$\begin{aligned} C = {} & \left[4b^3 \cos\theta \sin\theta - wb^2 (\cos\theta + 1)(3\cos\theta + 1) \right. \\ & \left. + 4bd^2 \sin\theta \right] (n_1 P_{t1} - n_2 P_{t2}) + (n_1 P_{t1} + 2n_2 P_{t2}) \\ & \cdot 8db^2 \cos\theta \sin\theta - 2db(\cos\theta - 1)(w + b\sin\theta) \\ & \cdot (2n_1 P_{t1} + n_2 P_{t2}) + 4wdb(2n_1 P_{t1} + n_2 P_{t2}) \\ & - \left(d^2 - 2db\cos\theta - 2b^2 \cos^2\theta \right) G, \end{aligned} \tag{15}$$

$$\begin{aligned} D = {} & \left[2wb^3 \cos\theta (\cos\theta + 1) + 2b^4 \sin\theta \cos^2\theta (\cos\theta - 1) \right] \\ & \cdot (n_1 P_{t1} + n_2 P_{t2}) + 8db^3 \sin\theta \cos^2\theta n_2 P_{t2} + (n_1 P_{t1} \\ & - n_2 P_{t2}) \left[4wdb^2 \cos\theta (\cos\theta + 1) + 4db^3 \cos\theta \sin\theta \right. \\ & \left. \cdot (\cos\theta - 1) \right] - 8d^2 b^2 \cos\theta \sin\theta n_2 P_{t2} - 2wdb^2 \\ & \cdot \left(\cos^2\theta - 1 \right) n_1 P_{t1} + 2wd^2 b(\cos\theta + 1) n_1 P_{t1} \\ & + 2d^2 b^2 \sin\theta (\cos\theta - 1) n_1 P_{t1} - \left(2bd^2 \cdot \cos\theta \right. \\ & \left. + 2db^2 \cdot \cos^2\theta \right) \cdot G, \end{aligned} \tag{16}$$

$$\begin{aligned} E = {} & wb^4 \cos^2\theta \left(\cos^2\theta - 1 \right) (n_1 P_{t1} - n_2 P_{t2}) - 4d^2 b^3 \cos^2\theta \\ & \cdot \sin\theta n_2 P_{t2} - 2db^3 \cos^2\theta (\cos\theta - 1)(w + b\sin\theta) n_2 P_{t2} \\ & + wdb^2 \left(\cos^2\theta - 1 \right) (2b\cos\theta + d) n_1 P_{t1} \\ & + 4wdb^3 \cos^2\theta n_2 P_{t2} - \left(d^2 b^2 \cos^2\theta + 2db^3 \cos^3\theta \right. \\ & \left. + b^4 \cos^4\theta \right) G. \end{aligned} \tag{17}$$

3.2.2. Error Compensation Model (ECM). On nonlinear identification problem of finite samples, the least square support vector regression (LSSVR) method gets desirable prediction effect. It has also attracted a lot of attention in industrial field.

In view of the advantages of LSSVR, the LSSVR model is selected to compensate the error between the prediction result of the mechanism model and the actual value. For detailed content, see the literature [17, 18].

3.3. Vibration State Flotation Height Prediction Model (VSFHP). At vibration state, the strip is usually reciprocating vibration around an equilibrium position. When the flotation height is too high or too low, the strip surface will be scratched due to contact with the nozzle. Therefore, in order to ensure the quality of the strip, accurately predicting the strip height is a key factor at vibration state. The LSSVR model is employed to predict the highest and lowest point of the strip during the vibration process.

In Figure 6, based on the experimental device, an online sensor is used to collect the flotation height experimental dataset $\{X^{\mathrm{V}}, Y^{\mathrm{V}}\}$ at vibration state, wherein X^{V} are features that affect the flotation height at vibration state and Y^{V} is the actual flotation height. The laser range finder is used to measure and record the flotation height of strip, and the maximum values $Y^{\mathrm{V}}_{\max}$ and the minimum value $Y^{\mathrm{V}}_{\min}$ during the vibration state are extracted by Matlab software. The datasets $\{X^{\mathrm{V}}, Y^{\mathrm{V}}_{\max}\}$ and $\{X^{\mathrm{V}}, Y^{\mathrm{V}}_{\min}\}$ are used to train the two LSSVR. Two LSSVR predict the maximum and minimum flotation height of the strip, respectively.

3.4. Flotation Height Prediction Frame Based on Hard Division Method. The flotation height prediction frame consists of division phase and prediction phase. The schematic diagram of the frame is shown in Figure 7.

In Figure 7, the procedure of the flotation height prediction frame is as follows:

(1) Division phase: the hard division model consists of the SDAE and FPKC method. Through practical experience and analysis, we can see that the state is related to fluid density, the impinging angle of slot nozzle, the nozzle pressure, the thickness of strip, and the density of strip. The goal of this phase is to accurately divide the stable state and vibration state of the strip and lay the foundation for the flotation height prediction of strip under stable state and vibration state.

(2) Prediction phase: based on the stable state and vibration state defined in division phase, the stable state and vibration state models are used to predict the flotation height. That is, the flotation height under stable state is predicted by the parallel hybrid prediction model in Section 3.2, and the LSSVR is used to predict the maximum and minimum flotation height under vibration state in Section 3.3.

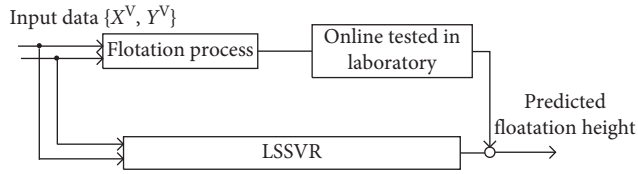

Figure 6: Vibration state flotation height prediction model schematic.

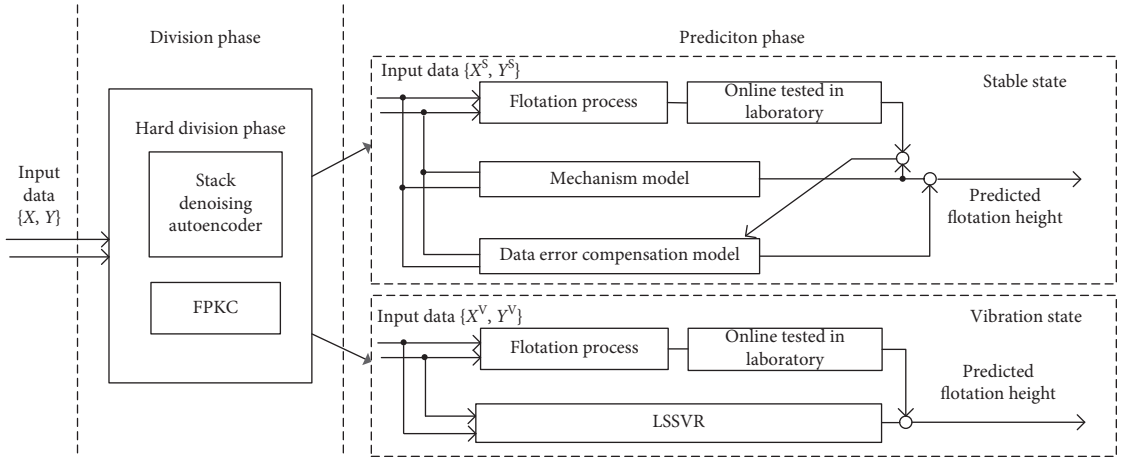

Figure 7: Flotation height prediction frame schematic diagram.

4. Experimental Results

4.1. Description of Test Device. The proposed frame is verified on the air flotation experimental platform developed by us. The schematic diagram and equipment figure of the air cushion furnace experimental platform are shown in Figures 8 and 9, respectively [1]:

The air flotation experimental platform includes furnace body, upper and lower fans, upper and lower air containers, upper and lower air boxes, upper and lower slot nozzles, air-seal devices, etc. The type of inverter in experimental platform is Siemens MM 440. The specification of the experimental platform is 3 m × 3 m × 2.2 m. The product type of laser range finder is LOD2-250W150 whose measurement accuracy and frequency are 75 μm and 1.33 kHz, respectively. It is just to facilitate the measurement and acquisition of data during the experiment. However, in the actual industrial process, laser range finder does not exist in the air cushion furnace. This experiment used strip with width of 300 mm. The strip thickness ranges from 0.4 mm to 2 mm. The same independent experiment was repeated four times under identical condition, and the average of the experimental results is used as the final result. The hard division method proposed in this paper is used to divide the dataset in the floating process into stable state dataset and vibration state dataset.

4.2. Experimental Setup. In order to train the hybrid model, we collected a total of 2050 strip floating samples covering eight working conditions. Among them, 630 stable state samples and 32 samples under 4 different states were collected to test the hybrid model. 1420 samples at vibration state were also collected, and 32 samples under 4 different vibration states were collected to test the hybrid model.

In practice, the interfering signal and instrumentation precision affect the quality of the collected data so that the precision of the model will be degraded. The statistics discriminant method of Pauta criteria is applied to eliminate abnormal data. The data are processed by Pauta criteria standard discriminant equations (18) and (19):

$$v_i = x_i - \overline{X}, \tag{18}$$

$$\sigma = \sqrt{\sum_{i=1}^{n}\left[\frac{v_i^2}{(n-1)}\right]}, \tag{19}$$

where $\overline{X}$ is the mean value of the sample data X and v_i, $i = 1, 2, \ldots, N$, represents the deviation between the original value and the mean value. If $|v_i| \geq 3\sigma$, eliminate the sample x_i. The parameters of the SDAE are given as follows: through the data preprocessing of the experimental data, the number of stacked layers is 2, and the number of hidden layer nodes of the first and second layer of SDAE is 15 and 10, respectively. The parameters of FPKC method are as follows: $d = 5$ Pa. In order to verify the superiority of SSPM, a lot of related validation experiments have been carried out. The experimental results of the proposed algorithm are compared with other algorithms, i.e., the mechanism model (MM), LSSVR, basic bagging (BB), and SBEH. The parameter setting of comparative algorithms is given as follows: in LSSVR, $\gamma = 4$, $\sigma^2 = 4025$; the number of weak classifiers in basic bagging hybrid model is 120.

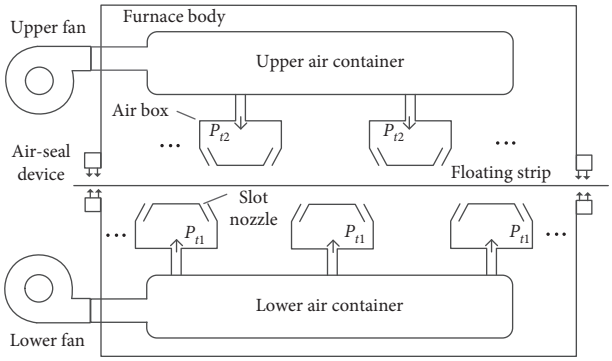

Figure 8: The schematic diagram of air flotation experimental platform.

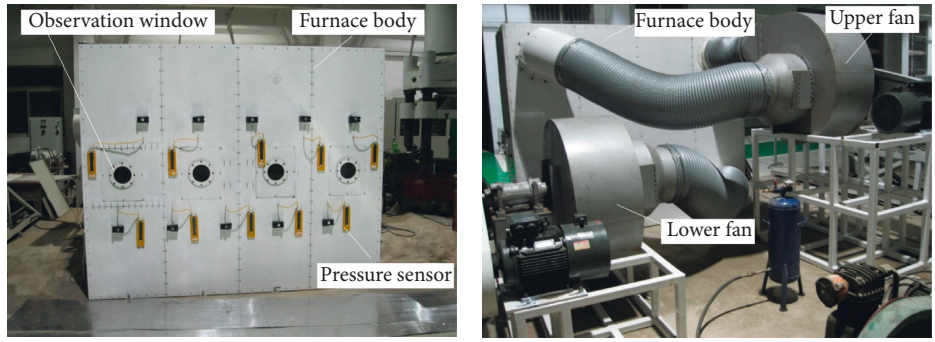

(a) (b)

Figure 9: Equipment figure of air flotation experimental platform. (a) Diagram of observation side of equipment. (b) Diagram of device operation side of equipment.

The evaluation indexes for model evaluation are RMSE, MAE, and MAPE. The equations are shown as follows:

$$\text{RMSE} = \sqrt{\frac{1}{N}\sum_{i=1}^{N}\left(Y_{o_i} - Y_{e_i}\right)^2}, \tag{20}$$

$$\text{MAE} = \frac{1}{N}\sum_{i=1}^{N}\left|Y_{o_i} - Y_{e_i}\right|^2, \tag{21}$$

$$\text{MAPE} = \sum_{i=1}^{N}\left|\frac{Y_{oi} - Y_{ei}}{Y_{oi}}\right| \times \frac{100}{N}, \tag{22}$$

where Y_o is actual flotation height and Y_e is the prediction value of flotation height.

4.3. Experimental Results and Analysis. This experiment was carried out on the air flotation experimental platform. In Figure 10, the width of the aluminum strip is 300 mm. When the thickness of strip is 1 mm and the pressure P_{t2} is 0 Pa and 40 Pa, respectively, the division results of stable state and vibration state are as shown in Figures 10(a) and 10(b). When the thickness of strip is 2 mm and the pressure P_{t2} is 0 Pa and 40 Pa, respectively, the division results are as shown in Figures 10(c) and 10(d).

In Figure 10(a), when $0 \le t \le 4.6$ s, $P_{t1} = 300$ Pa, and $P_{t2} = 0$ Pa, the strip is at stable state. When $4.7 \le t \le 11$ s, $P_{t1} = 360$ Pa, and $P_{t2} = 0$ Pa, the strip is at vibration state. In vibration state, the maximum value and minimum value of flotation height are about 31 mm and 25 mm, respectively. The hard division algorithm divides the flotation state into stable state and vibration state at the time of $t = 4.6$ s.

In Figure 10(b), when $0 \le t \le 4.7$ s, $P_{t1} = 320$ Pa, and $P_{t2} = 40$ Pa, the strip is under stable state. When $4.6 \le t \le 11$ s, $P_{t1} = 380$ Pa, and $P_{t2} = 40$ Pa, the strip is under vibration state. In stable state, the maximum value of flotation height is about 39 mm and the minimum value of flotation height is about 29 mm. The hard division algorithm divides the flotation state into stable state and vibration state at the time of $t = 4.7$ s.

In Figure 10(c), when $0 \le t \le 5.0$ s, $P_{t1} = 360$ Pa, and $P_{t2} = 0$ Pa, the strip is at stable state. When $5.1 \le t \le 11$ s, $P_{t1} = 420$ Pa, and $P_{t2} = 0$ Pa, the strip is at vibration state. In vibration state, the maximum value and minimum value of flotation height are about 29 mm and 23 mm, respectively. The hard division algorithm divides the flotation state into stable state and vibration state at the time of $t = 5.1$ s.

In Figure 10(d), when $0 \le t \le 4.7$ s, $P_{t1} = 400$ Pa, and $P_{t2} = 40$ Pa, the strip is under stable state. When $4.8 \le t \le 11$ s, $P_{t1} = 470$ Pa, and $P_{t2} = 40$ Pa, the strip is under vibration state. In vibration state, the maximum value of flotation height is about 24 mm and the minimum value of flotation

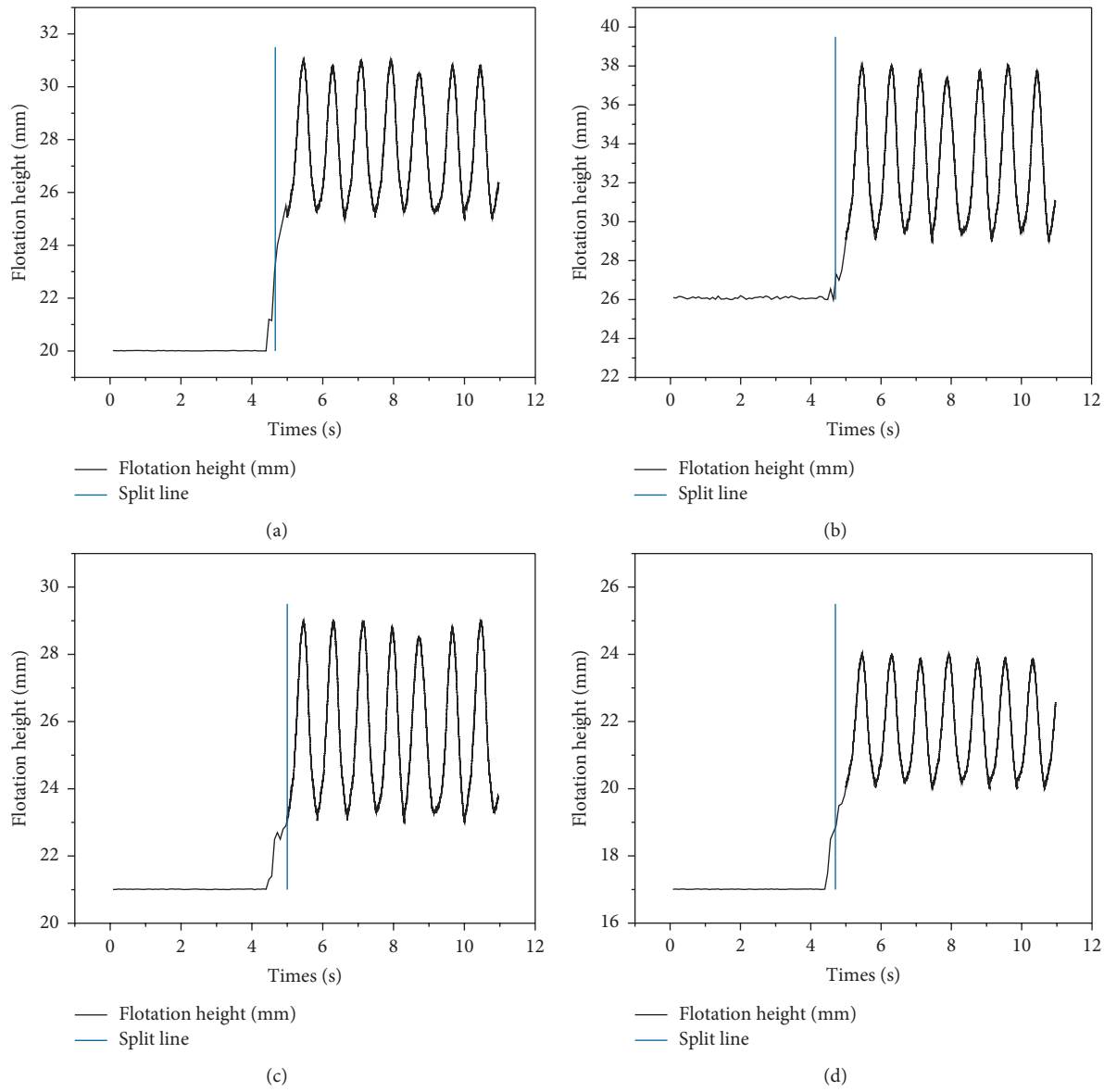

Figure 10: The phase division results in air flotation process under stable state and vibration state. (a) Thickness = 1 mm; upper pressure = 0 Pa. (b) Thickness = 1 mm; upper pressure = 40 Pa. (c) Thickness = 2 mm; upper pressure = 0 Pa. (d) Thickness = 2 mm; upper pressure = 40 Pa.

height is about 20 mm. The hard division algorithm divides the flotation state into stable state and vibration state at the time of $t = 4.7$ s.

We compare our proposed method with SBEH, LSSVR, bagging, and MM. The stable experimental results are shown in Figure 11. When the thickness of strip is 1 mm and the pressure P_{t2} is 0 Pa and 40 Pa, respectively, the relationship between flotation height and P_{t1} is as shown in Figure 11(a) and Figure 11(b). When the thickness of strip is 2 mm and the pressure P_{t2} is 0 Pa and 40 Pa, respectively, the relationship between flotation height and P_{t2} is as shown in Figure 11(c) and Figure 11(d).

In Figure 11, the effects of these five algorithms are compared. SSPM has preferable generalization ability and accuracy. For the reader's convenience, Table 1 shows the RMSE, MAE, and MAPE of these five algorithms.

In Table 1, SSPM has got better prediction results than SBEH. The reason can be explained by the fact that the simplified mechanism part of SSPM and SBEH is established based on thick-wall jet theory and thin-wall jet theory, respectively. The thick-wall theory is more suitable for the circumstance of low flotation height. The flotation height is low when the strip is under stable state, so the simplified mechanism part of SSPM is more suitable for the prediction of stable state. SSPM and SBEH get better prediction results than LSSVR, bagging, and MM. The reason may be that the generalization ability of the data-driven model is poor and the mechanism model is established based on the ideal

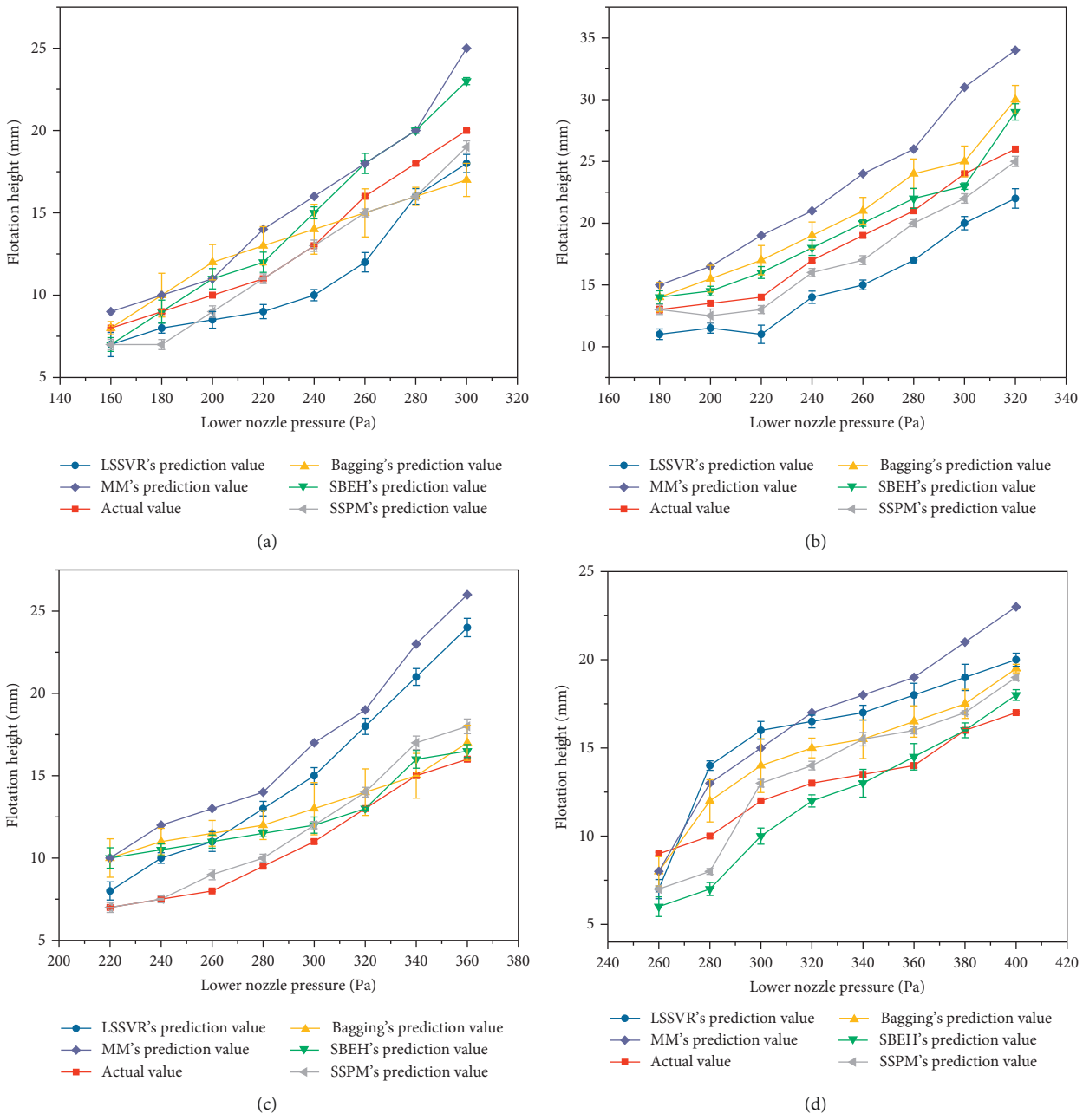

Figure 11: The prediction and actual flotation height under stable state. (a) Thickness = 1 mm; upper pressure = 0 Pa. (b) Thickness = 1 mm; upper pressure = 40 Pa. (c) Thickness = 2 mm; upper pressure = 0 Pa. (d) Thickness = 2 mm; upper pressure = 40 Pa.

Table 1: Flotation height prediction results of different algorithms at stable state.

	P_{t2}	Strip thickness = 1 mm					Strip thickness = 2 mm				
		MM	LSSVR	Bagging	SBEH	SSPM	MM	LSSVR	Bagging	SBEH	SSPM
RMSE	0 Pa	2.598	2.271	1.732	1.732	**1.225**	6.230	4.603	2.391	2.039	**1.186**
	40 Pa	5.208	3.298	2.449	1.541	**1.275**	4.202	3.437	1.992	1.750	**1.696**
MAE	0 Pa	2.250	2.063	1.500	1.500	**1.000**	5.875	4.125	2.063	1.688	**1.250**
	40 Pa	4.875	3.125	2.250	1.375	**1.125**	3.938	3.375	1.938	1.375	**1.625**
MAPE	0 Pa	16.571	15.748	11.168	10.698	**8.385**	25.864	17.678	12.508	7.625	**5.988**
	40 Pa	53.657	35.848	23.964	20.037	**7.547**	29.059	17.525	14.989	18.528	**13.170**

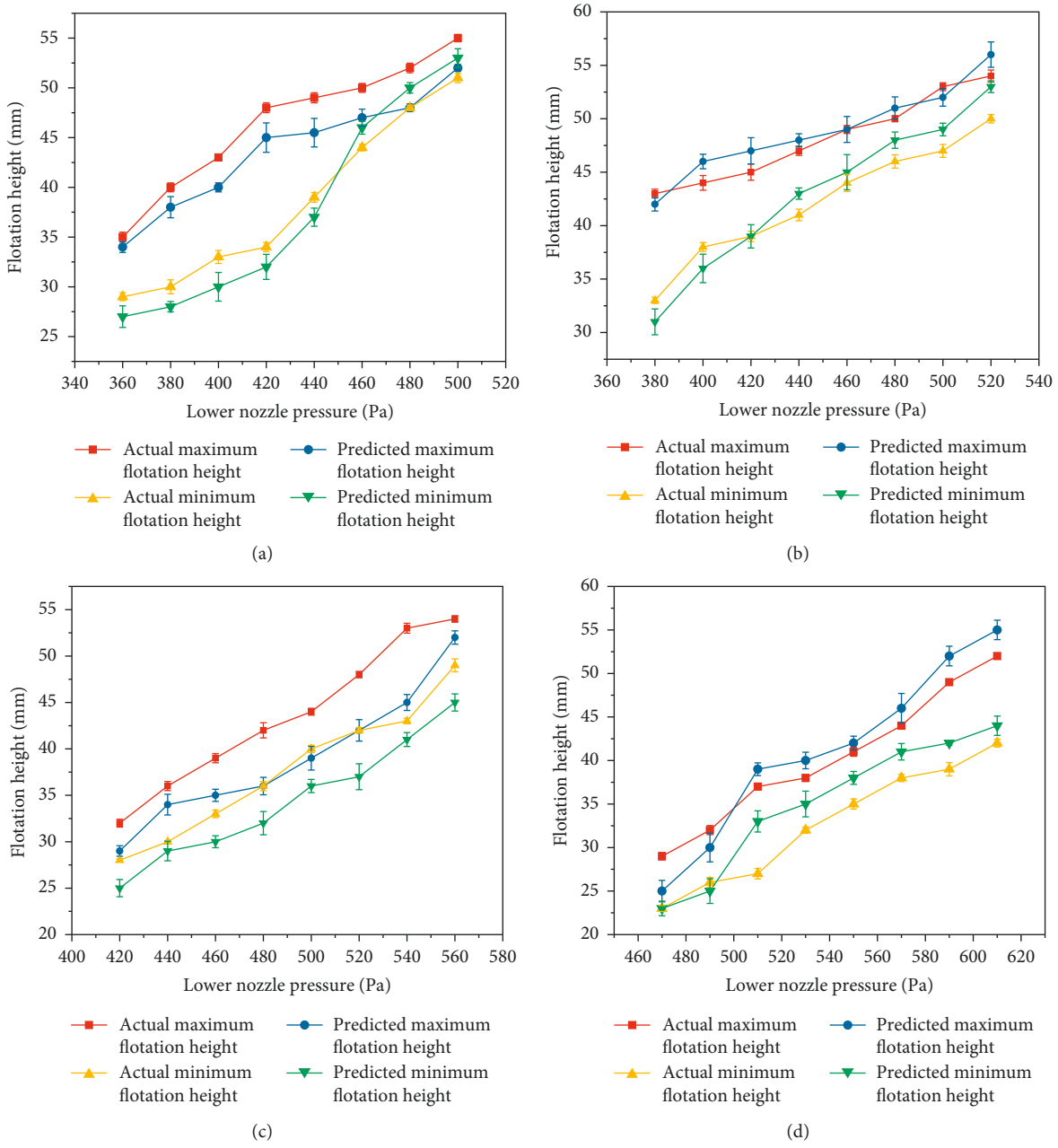

FIGURE 12: The maximum and minimum flotation height at vibration state. (a) Thickness = 1 mm; upper pressure = 0 Pa. (b) Thickness = 1 mm; upper pressure = 40 Pa. (c) Thickness = 2 mm; upper pressure = 0 Pa. (d) Thickness = 2 mm; upper pressure = 40 Pa.

hypothesis which ignores the coupling process between the flow fields. The hybrid parallel model combines the advantage of strong learning ability of the data-driven model and the high generalization of mechanism model. The data-driven model can compensate the unmodeled part and difficult modeling part of the mechanism model.

Moreover, it can be found that prediction effect of bagging is superior to LSSVR. The reason is that Bagging integrates multiple weak leaners, so bagging has higher generalization and diversity than single LSSVR. Bagging and LSSVR are superior to the mechanism model. The reason may be as follows: the strip flotation process is a fluid solid coupling process between the strip and air. The fluid solid coupling process is hard to be established by the mechanism model. The mechanism model is established based on the ideal hypothesis that the effect of coupling process between the flow fields can be ignored. Bagging and LSSVR with the advantage of strong learning ability can compensate the unmodeled part and difficult modeling part of the mechanism model. So the data-driven model is easy to get better prediction results than mechanism.

The vibration experimental results are shown in Figure 12. When the thickness of strip is 1 mm and the pressure P_{t2} is 0 Pa and 40 Pa, respectively, the relationship between maximum and minimum flotation height and P_{t1} is as shown in Figures 12(a) and 12(b), respectively. When the

Table 2: Prediction results of maximum and minimum flotation height at vibration state.

	P_{t2}	Strip thickness = 1 mm		Strip thickness = 2 mm	
		Predicted maximum height	Predicted minimum height	Predicted maximum height	Predicted minimum height
RMSE	0 Pa	2.942	2.151	4.924	3.464
	40 Pa	1.414	1.936	2.520	3.102
MAE	0 Pa	2.813	2.125	4.500	3.250
	40 Pa	1.250	1.750	2.375	2.625
MAPE	0 Pa	5.922	5.787	10.269	8.621
	40 Pa	2.629	4.135	6.199	8.046

thickness of strip is 2 mm and the pressure P_{t2} is 0 Pa and 40 Pa, respectively, the relationship between maximum and minimum flotation height and P_{t2} is as shown in Figures 12(c) and 12(d), respectively.

According to experiment results in the vibration state shown in Table 2, high accuracy can be obtained by using LSSVR to predict maximum and minimum value of flotation height. The reason is that LSSVR owns strong learning ability and can learn the information in fluid and solid coupling process. LSSVR can get better prediction results under the circumstance that the training samples is few.

The proposed method can be applied to not only the flotation height prediction of the 1 mm and 2 mm strip in the air cushion furnace but also the flotation height prediction of other standard specifications of the strip. The reasons are as follows. Firstly, there are two work states in the production process. The hard division method proposed can divide the flotation state into stable state and vibration state. The division method can also be applied to other specifications of the strip. Secondly, the mechanism model based on the thick-wall jet theory has better prediction capability, when the strip is under a stable state. In addition, the data-driven model is used to compensate output error between the output of mechanism model and the actual value. The data-driven model has better learning ability and can mine the valuable information from the process data. The hybrid model consisted of the mechanism model and data-driven model. The above two factors let the hybrid model combine the good generalization performance of the mechanism model and strong learning ability of data model, so the proposed hybrid model can also be applied to flotation height prediction of other specifications strip. Thirdly, when the strip is under the vibration state, the data-driven model is used to predict the minimum value and the maximum value of the flotation height. The data-driven model has better fitting capacity for the vibration state data. It can also be used for the prediction of other specifications of the strip. In summary, the SSPM proposed can predict flotation height to the other specifications of the strip.

5. Conclusions

In this paper, the content of study is flotation height prediction framework under stable state and vibration state. The flotation height prediction frame based on the hard division method is proposed in this paper. The main conclusions are as follows:

(1) In this paper, the flotation height prediction framework based on the hard division method is proposed. This method can divide the working state into stable state and vibration state and output flotation height values both at stable state and vibration state accurately.

(2) A hard division method based on stacked denoising autoencoder and FPKC method is proposed. A FPKC algorithm which combines the knowledge of flotation process is established and can be applied for the time continuity problem. This hard division method can divide the working condition into stable state and vibration state with high precision.

(3) A parallel hybrid flotation height model SSPM for stable state is proposed. The SSPM gets better prediction results than SBEH, bagging, LSSVR, and MM methods. Compared with SBEH, SSPM established based on thick-wall jet theory is more suitable for the situation of low flotation height. The reason why the prediction effect of SSPM is better than LSSVR, bagging, and MM methods is that the SSPM combines the strong learning ability of the data-driven model and generalization of the mechanism model.

(4) Finally, according to the vibration characteristics of strip in air cushion furnace, LSSVR is used to predict the maximum and minimum flotation height of the strip under vibration state. The vibration state prediction model has achieved good prediction results.

Data Availability

The data used to support the findings of this study are available from the corresponding author upon request.

Conflicts of Interest

The authors declare that there are no conflicts of interest regarding the publication of this article.

Acknowledgments

This study was supported by the Fundamental Research Funds for the Central Universities of China under Project no. N180708009, Collaborative Innovation Center of Steel Technology Open Subject (no. 2015001), Natural Science Foundation of Hebei Province of China (no. E2017402115).

The authors also thank Zhang Xinyuan, Han Xiaolin, and Liu Jitong for assistance in the study.

References

[1] S. Hou, F. Hua, W. LV, Z. Wang, Y. Liu, and G. Wang, "Hybrid modeling of flotation height in air flotation oven based on selective bagging ensemble method," *Mathematical Problems in Engineering*, vol. 2013, Article ID 281523, 9 pages, 2013.

[2] S. Hou, X. Wang, F. Hua et al., "Research and development of the test platform for large air flotation type Annealing furnaces," *Journal of Northeastern University (Natural Science)*, vol. 36, no. 12, pp. 1706–1709, 2015.

[3] X. Wang, M. Guo, L. Cao, J. Luo, J. Zhang, and L. Zhuang, "Effect of heating rate on mechanical property, microstructure and texture evolution of Al-Mg-Si-Cu alloy during solution treatment," *Materials Science and Engineering: A*, vol. 621, pp. 8–17, 2015.

[4] Y. Li, J. Li, X. Ling et al., "Optimization and aerodynamic characteristics of new air-cushion nozzle of floating furnace for automobile body sheet," *Journal of Harbin Institute of Technology (New Series)*, vol. 24, no. 1, pp. 57–64, 2017.

[5] W. Zhao, D. Liu, Q. Feng, S. Wen, and W. Chang, "DFT insights into the electronic properties and adsorption mechanism of HS− on smithsonite (1 0 1) surface," *Minerals Engineering*, vol. 141, p. 105846, 2019.

[6] Q. Feng, S. Wen, X. Bai, W. Chang, C. Cui, and W. Zhao, "Surface modification of smithsonite with ammonia to enhance the formation of sulfidization products and its response to flotation," *Minerals Engineering*, vol. 137, pp. 1–9, 2019.

[7] L. Yong, W. Zhaodong, M. Mingtu et al., "Air cushion furnace technology for heat treatment of high quality aluminum alloy auto body sheet," *Engineering Sciences*, vol. 12, no. 5, pp. 73–80, 2014.

[8] T. Huang, P. Tan, M. Li, Y. Zhang, and H. Zhou, "Numerical modeling and analysis of heat transfer for floatation nozzle with a flexible substrate," *International Journal Of Thermal Sciences*, vol. 137, pp. 665–674, 2019.

[9] S. S. Chen, W. H. Chen, J. M. Liu et al., "An aerostatic bearing device with arrayed restrictors for roll-to-roll printed electronics," in *Proceedings of the 14th International Conference on Control, Automation, Robotics And Vision*, Phuket, Thailand, November 2016.

[10] Y. B. Chang and P. M. Moretti, "Aerodynamic characteristics of pressure-pad air bars," *Journal of Applied Mechanics*, vol. 67, no. 1, pp. 177–182, 2000.

[11] W. X. Chen, Y. H. He, F. S. Liu et al., "Analysis and test of floating height of air cushion plate strip," *Journal of the Southern African Institute of Mining and Metallurgy*, vol. 3, pp. 251–259, 1989.

[12] P. M. Moretti, "Lateral deflections of Webs in air-flotation ovens," *Journal of Applied Mechanics*, vol. 71, no. 3, pp. 314–320, 2004.

[13] H.-K. Cho, *Flow-induced Vibration of a Web Floating over a Pressure-Pad Air bar*, Oklahoma State University, Stillwater, OK, USA, 2005.

[14] M. Takeda and M. Watanabe, "Self-excited vibration of a plate supported by air pressure in a floating conveying machine," in *Proceedings of the ASME 2017 Pressure Vessels and Piping Conference*, Waikoloa, HI, USA, July 2017.

[15] L. Jiang, Z. Song, Z. Ge, and J. Chen, "Robust self-supervised model and its application for fault detection," *Industrial & Engineering Chemistry Research*, vol. 56, no. 26, pp. 7503–7515, 2017.

[16] R. C. Deo, M. K. Tiwari, J. F. Adamowski, and J. M. Quilty, "Forecasting effective drought index using a wavelet extreme learning machine (W-ELM) model," *Stochastic Environmental Research and Risk Assessment*, vol. 31, no. 5, pp. 1211–1240, 2017.

[17] Y. Qin, C. Zhao, and F. Gao, "An iterative two-step sequential phase partition (ITSPP) method for batch process modeling and online monitoring," *AIChE Journal*, vol. 62, no. 7, pp. 2358–2373, 2016.

[18] C. Zhao, "Concurrent phase partition and between-mode statistical analysis for multimode and multiphase batch process monitoring," *AIChE Journal*, vol. 60, no. 2, pp. 559–573, 2014.

[19] R. Stewart and S. Ermon, "Label-free supervision of neural networks with physics and domain knowledge," in *Proceedings of the Thirty-First AAAI Conference on Artificial Intelligence*, pp. 1–7, San Francisco, CA, USA, February 2017.

[20] J. Wang, Y. Chen, S. Hao et al., "Deep learning for sensor-based activity recognition: a survey, pattern recognition letters," 2018, http://arxiv.org/abs/1707.03502.

[21] H. Ren, R. Stewart, J. Song et al., "Learning with weak supervision from physics and data-driven constraints," *AI Magazine*, vol. 39, no. 1, pp. 1–12, 2018.

[22] W. Hu, R. R. Singh, and R. T. Scalettar, "Discovering phases, phase transitions, and crossovers through unsupervised machine learning: a critical examination," *Physical Review E*, vol. 95, no. 6, p. 062122, 2017.

[23] W. Y. Deng, Y. T. Qu, and Q. Zhang, "Domain adaption based on ELM autoencoder," *Mathematical Problems In Engineering*, vol. 46, no. 5, pp. 857–860, 2018.

[24] M. Gong, H. Yang, and P. Zhang, "Feature learning and change feature classification based on deep learning for ternary change detection in SAR images," *ISPRS Journal of Photogrammetry and Remote Sensing*, vol. 129, pp. 212–225, 2017.

[25] D. Xu, Y. Yan, E. Ricci, and N. Sebe, "Detecting anomalous events in videos by learning deep representations of appearance and motion," *Computer Vision and Image Understanding*, vol. 156, pp. 117–127, 2017.

[26] S. F. Hussain and M. Haris, "A k-means based co-clustering (kCC) algorithm for sparse, high dimensional data," *Expert Systems with Applications*, vol. 118, pp. 20–34, 2019.